SCIENCE CHINA Materials ARTICLES

mater.scichina.com link.springer.com

Published online 22 October 2019 | https://doi.org/10.1007/s40843-019-1193-x
*Sci China Mater* 2019, 62(12): 1821–1830

SPECIAL TOPIC: Dedicated to the 70th Birthday of Professor Kenneth R. Poeppelmeier

# $Ag_4Hg(SeO_3)_2(SeO_4)$: a novel SHG material created in mixed valent selenium oxides by *in situ* synthesis

Xiao-Xue Wang[1,2], Xiao-Bao Li[1,2], Chun-Li Hu[2], Fang Kong[2*] and Jiang-Gao Mao[2*]

**ABSTRACT** **Explorations of new second harmonic generation materials in $Ag^+$-$Hg^{2+}$/$Bi^{3+}$-selenites systems afforded three new silver selenium oxides, namely, $Ag_4Hg(SeO_3)_2(SeO_4)$ (1), $Ag_2Bi_2(SeO_3)_3(SeO_4)$ (2) and $Ag_5Bi(SeO_3)_4$ (3). They exhibit flexible crystal chemistry. Compounds 1 and 2 are mixed valence selenium oxides containing Se(IV) and Se(VI) cations simultaneously. Compounds 1 and 3 exhibit a 3D open framework with 4-, 6- and 8-member polyhedral ring tunnels along *a*, *b* and *c* axes. Compound 1 crystallized in a polar space group and could display a subtle frequency doubling efficiency about 35% of the commercial $KH_2PO_4$ (KDP). UV-vis-NIR spectra reveal that compounds 1–3 are wide-band semiconductors with the optical bandgaps of 3.11, 3.65, 3.58 eV respectively. Theoretical calculations disclose that compounds 2 and 3 are indirect band gap structures and their bandgaps are determined by Ag, Bi, Se and O atoms together.**

**Keywords:** SHG material, *in situ* synthesis, mixed valence selenium oxide, selenite

## INTRODUCTION

Design and syntheses of noncentrosymmetric (NCS) structures have received widespread attention due to their valuable physical properties, such as ferroelectric, pyroelectricity, piezoelectricity and second harmonic generation (SHG), which cannot be found in centrosymmetric (CS) compounds [1–4]. Selenites are a kind of important lone-pair oxyanions, of which the coordination environments are inherently polar, with the oxygen ligands situated at one side of the cations, due to the stereoactive nonbonded electron pair [5–7]. Selenite-based SHG materials, such as $Cs_2(MoO_3)_3(SeO_3)$ [8] ($P6_3$, 350 × α-$SiO_2$), $Zn_2(MoO_4)(SeO_3)$ [9] ($P2_1$, 100 × α-$SiO_2$), $Pb_2TiOF(SeO_3)_2Cl$ [10] ($P2_1$, 9.6 × KDP), $BiFSeO_3$ [11] ($Pca2_1$, 13.5 × KDP), $Pb_2GaF_2(SeO_3)_2Cl$ [12] ($P2_1$, 4.5 × KDP), and $PbCdF(SeO_3)(NO_3)$ [13] ($Pca2_1$, 2.6 × KDP), have been reported constantly. Most of them are mixed-anion compounds [14–17]. The second NCS functional units, such as $d^0$ transition metals, lone-pair cations, and π-conjugate planar units, have been incorporated into the metal selenites to enhance the comprehensive performance of the SHG materials.

Tetrahedral units, which are also NCS, have got our attention. We have introduced $BO_4$, $GaO_4$ and $SO_4$ tetrahedra into metal selenites or tellurites respectively [18]. The first boroselenite of $B_2Se_2O_7$ [19] ($P2_12_12_1$, 2.2 × KDP), α-gallium tellurite of $Ga_2(TeO_3)_3$ [20] ($I$-43$d$, 1.0 × KDP) and indium sulfate tellurite of $In_3(SO_4)(TeO_3)_2F_3(H_2O)$ [21] ($P2_12_12_1$, 0.11 × KDP) were isolated successfully. As we know, hexavalent Se and tetravalent S behave similarly in coordination mode [17,22]. They prefer NCS tetrahedral geometry when coordinated with oxygen atoms. So, mixed-valence selenite-selenates are such compounds in which polar triangular pyramidal Se(IV)$O_3$ and NCS tetrahedral Se(VI)$O_4$ exist simultaneously [23–32]. Based on the literature research, we found the reported inorganic selenite-selenate compounds are still rare. And only $Au_2(SeO_3)_2(SeO_4)$ [26] ($Cmc2_1$, 0.43 × KDP) was studied by SHG measurements although six mixed-valent selenium oxides were crystalized in NCS space group [23–28].

Most of the reported selenite-selenate compounds were prepared by *in situ* syntheses [23–32]. The mixed-valent selenium atoms were achieved by partial reduction of the hexavalent selenic acid or oxidation of the tetravalent selenium dioxide. It is not easy to gain mixed-valent se-

[1] College of Chemistry, Fuzhou University, Fuzhou 350108, China
[2] State Key Laboratory of Structural Chemistry, Fujian Institute of Research on the Structure of Matter, Chinese Academy of Sciences, Fuzhou 350002, China
[*] Corresponding authors (emails: Kongfang@fjirsm.ac.cn (Kong F); mjg@fjirsm.ac.cn (Mao JG))

  

lenium oxides due to the uncontrolled reduction or oxidation process. If partial reduction or oxidation failed, pure selenites or selenates were obtained. To partially oxidize selenium dioxide, oxidant of $Ag^{+}$ was used, which can also be used as the balance cations [33,34]. Furthermore, $d^{10}$ transition metal of $Hg^{2+}$ and lone-pair cation of $Bi^{3+}$ were also introduced into silver-selenite-selenates, respectively [35–37]. No structures were reported in this area. Our efforts in $Ag^{+}$-$Hg^{2+}$/$Bi^{3+}$-$SeO_3$-$SeO_4$ systems afford three new silver selenite-selenates, namely, $Ag_4Hg(SeO_3)_2(SeO_4)$ (**1**), $Ag_2Bi_2(SeO_3)_3(SeO_4)$ (**2**) and $Ag_5Bi(SeO_3)_4$ (**3**). They exhibit flexible crystal chemistry. Compound **1** is crystallized in NCS space group while compounds **2** and **3** are centrosymmetric. Herein, we will report their syntheses, structures, and optical properties in detail.

## EXPERIMENTAL SECTION

### Materials and instruments

All the reagents were obtained from commercial sources and employed without further refinement: $AgNO_3$ (99.8%, AR), $Bi_2O_3$ (>99.5%, AR), $Bi(NO_3)_3{\cdot}5H_2O$ (>99%, AR), HgO (>99%, AR) and $SeO_2$ (>99%, AR). Powder X-ray diffraction (XRD) patterns were collected on a Rigaku MiniFlex II diffractometer using Cu-Kα radiation in the angular range of $2\theta$ = 10°–70° with a step size of 0.02° at 293 K. Microprobe elemental analyses were done with the field-emission scanning election microscopy (FESEM, JSM67F) equipped with an energy-dispersive X-ray spectroscopy (EDS, Oxford INCA). IR spectrum was carried out on a Magna 750 FT-IR spectrometer using air as background in 4000–400 $cm^{-1}$ with a resolution of 2 $cm^{-1}$. The UV-vis-NIR spectrum was collected at 250–2500 nm by a PerkinElmer Lambda 900 spectrophotometer using $BaSO_4$ as a reference, and the reflection spectrum was converted into an absorption spectrum using the Kubelka-Munk function. The thermogravimetric analyses (TGA) were performed on a Netzsch STA 449C analyzer with heating rate of 10°C/min under $N_2$ atmosphere from 25 to 1000°C. SHG efficiency was measured by the reported method [38]. The fundamental wavelength is 1064 nm produced by a Q-switched Nd:YAG laser. Sieved KDP crystals (70–100 mesh) were used as the reference.

### Synthesis

Single crystals of compounds **1**–**3** were obtained through mild hydrothermal method. Mixed-valence selenium compounds of **1** and **2** were synthesized directly by *in-situ* reactions. The starting materials are HgO (0.2 mmol), $AgNO_3$ (0.8 mmol), $SeO_2$ (1.0 mmol) for compound **1**; $Bi_2O_3$ (0.25 mmol), $Bi(NO_3)_3{\cdot}5H_2O$ (0.5 mmol), $AgNO_3$ (1.0 mmol), $SeO_2$ (2.0 mmol) for **2** and **3**. The mixtures and 3 mL deionized water were loaded in 23 mL Teflon-lined autoclaves, which were heated to 230°C (180°C for **3**) to generate autogenous pressures in 6 h and held for 4 days, followed by cooling to 30°C at a rate of 3°C/h. The resultants of reactions were filtered from the mother liquor, and washed thoroughly with deionized water, then dried at room temperature. Pure phases of **1** (yellow blocks), **2** (light yellow rods) and **3** (orange blocks) were collected in ca. 56%, 75% and 69% yields (based on Ag), respectively (Fig. S1, see Supplementary information). Their purities were checked by powder XRD. Fig. S2 shows that the measured patterns are in coincidence with the calculated ones, indicating that the samples are single phases.

It is worth noting that partial $Se^{4+}$ reagents were oxidized to $Se^{6+}$ in compounds **1** and **2** while no oxidation reaction occurred in compound **3**. Based on comparison of the reaction conditions, we found two factors may cause the formation of mixed-valence selenium structures by *in-situ* reactions. The first one is the relatively high reaction temperature (such as 230°C), which can be discovered in the reactions of compounds **2** and **3**. The same starting materials reacting at different temperatures result in different structures. Higher temperature yields mixed-valence compound of **2**, while lower temperature brings out pure selenite of **3**. The other is the existence of the strong oxidants of $Ag^{+}$ and $HNO_3$, which were formed in the acidic solvent of $SeO_2$. The synergy of high temperature and strong oxidant give rise to the construction of mixed-valence selenium oxides of **1** and **2**.

### Single crystal structure determination

Single crystal XRD data of the three compounds were collected at 273 K by using Agilent Technologies SuperNova dual wavelength CCD diffractometer with graphite-monochromatic Mo-Kα radiation ($\lambda$ = 0.77103 Å). Date reduction was completed with the CrysAlisPro program. The absorption correction was achieved by multi-scan method [39]. The structures were determined through the direct method and refined by full-matrix least-squares fitting on $F^2$ relying on SHELXL-97 [40], and also checked by PLATON for possible missing symmetry elements [41]. For compound **1**, the Ag(1) site is disordered and mixed with Hg(1) atom. Their occupancies were refined as 0.5:0.5 based on the charge neutrality principle, which were also confirmed by the EDS ele-

  

mental analyses (Fig. S3). Crystallographic data and structural refinements for the crystals are summarized in Table 1. Important bond distances are listed in Table S1.

### Computational method

The theoretical calculations of compounds **2** and **3** were based on their single crystal structure data. The electronic structures were obtained in the computer code of CASTEP by using the first principle plane wave and pseudo potential based on the density functional theory (DFT) [42]. As for the exchange and correlation functions, we selected Perdew-Burke-Ernzerhof (PBE) in the generalized gradient approximation (GGA). The interaction between the nucleus and electrons was demonstrated using a norm-conserving pseudopotential. The following orbital electrons were considered to be the valence electrons of each element: Ag-$4p^6 4d^{10} 5s^1$, Bi-$5d^{10} 6s^2 6p^3$, Se-$4s^2 4p^4$, O-$2s^2 2p^4$. The numbers of plane waves included in the basis sets were determined by a cutoff energy of 765 eV for compounds **2** and **3**. The numerical integration of the Brillouin zone was performed using a Monkhorst-Pack *k*-point sampling of 3 × 5 × 2 and 3 × 3 × 3 for compounds **2** and **3**, respectively.

## RESULTS

### Crystal structure of $Ag_4Hg(SeO_3)_2(SeO_4)$ (1)

$Ag_4Hg(SeO_3)_2(SeO_4)$ (**1**) crystallizes in orthorhombic space group $Cmc2_1$ (No. 36), which is NCS and polar. It features a 3D framework composed of silver/mercury selenite layers bridged by $SeO_4$ tetrahedra with silver situated in the space of the structure (Fig. 1). There are two silver, one mercury/silver, three selenium and seven oxygen atoms, totaling 13 unique atoms in its asymmetric unit. The mixed Ag/Hg(1) cation was linked with six oxygen atoms in an octahedral geometry with the coordination bond lengths in the range of 2.380(17)–2.61(2) Å (Fig. S4). Ag(2) and Ag(3) are connected with four and six oxygen atoms respectively, forming $Ag(2)O_4$ tetrahedron and $Ag(3)O_6$ triangular prism with the Ag–O distances in the range of 2.246(19)–2.73(2) Å (Fig. S5). Se(1) and Se(2) are in the $SeO_3$ triangular pyramidal geometries with Se–O bond lengths within 1.645(19)–1.732(18) Å while Se(3) is in a $SeO_4$ tetrahedral coordination with the Se–O bonds limited in 1.62(2)–1.65(2) Å (Fig. S6), which are consistent with the reported selenium oxides [8–13]. The Bond-valence-sum (BVS) calculation results of Ag/Hg(1), Ag(2), Ag(3), Se(1), Se(2) and Se(3) cations are 1.28, 0.96, 0.63, 4.0, 4.37, 6.09 (Table S2), respectively, proving that the oxidation states of Hg(1), Ag(1)–Ag(3), Se(1)–Se(2) and Se(3) are +2, +1, +4 and +6, respectively [43,44]. The deviation of Ag/Hg(1) from the ideal oxidation is mainly due to the low BVS of Ag atom, which is common in silver oxides [45–49]. The slightly higher valence for Se(2) can be attributed to the two short Se–O bonds (1.645 Å). $Ag_4Hg(SeO_3)_2(SeO_4)$ (**1**)

**Table 1** Summary of crystal data and structural refinements for the three compounds

| Formula | $Ag_4Hg(SeO_3)_2(SeO_4)$ | $Ag_2Bi_2(SeO_3)_3(SeO_4)$ | $Ag_5Bi(SeO_3)_4$ |
|---|---|---|---|
| FW | 1028.95 | 1157.54 | 1256.17 |
| Crystal system | Orthorhombic | Monoclinic | Tetragonal |
| Space group | $Cmc2_1$ | $P2_1/m$ | $I4_1/a$ |
| $a$ (Å) | 8.1690(9) | 9.5380(4) | 12.1616(2) |
| $b$ (Å) | 11.9903(14) | 5.4965(2) | 12.1616(2) |
| $c$ (Å) | 10.8870(14) | 11.8207(5) | 9.1293(3) |
| $\alpha$ (°) | 90 | 90 | 90 |
| $\beta$ (°) | 90 | 92.892(4) | 90 |
| $\gamma$ (°) | 90 | 90 | 90 |
| $V$ (°) | 1066.4(2) | 618.92(4) | 1350.27(5) |
| Z | 4 | 2 | 4 |
| $D_{calc}$ (g cm$^{-3}$) | 6.409 | 6.211 | 6.179 |
| *Flack* | 0.37(3) | | |
| $M$ (mm$^{-1}$) | 31.845 | 43.296 | 30.936 |
| GOF on $F^2$ | 1.132 | 1.051 | 1.038 |
| $R_1$, $wR_2[I>2\sigma(I)]$[a] | 0.0417, 0.1171 | 0.0393, 0.0728 | 0.0323, 0.0788 |
| $R_1$, $wR_2$(all data)[a] | 0.0423, 0.1177 | 0.0466, 0.0790 | 0.0356, 0.0819 |

a) $R_1 = \sum||F_o| - |F_c||/\sum|F_o|$, $wR_2 = \{\sum w[(F_o)^2 - (F_c)^2]^2/\sum w[(F_o)^2]^2\}^{1/2}$

  

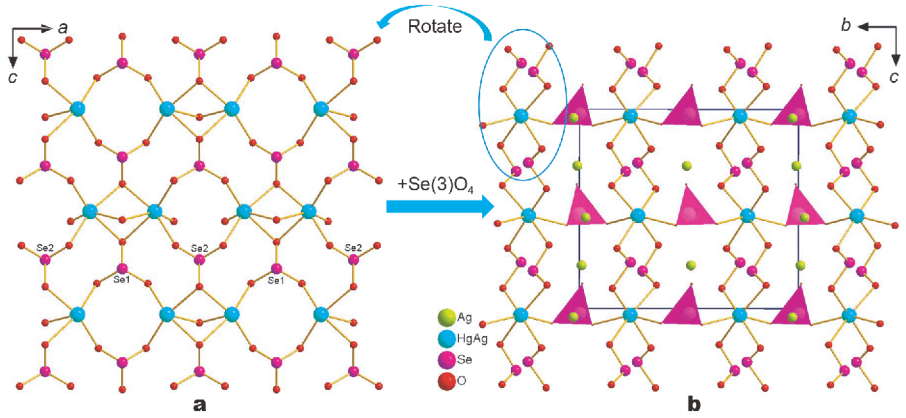


**Figure 1** The 2D silver/mercury selenite layer (a) and the structure of $Ag_4Hg(SeO_3)_2(SeO_4)$ (**1**) along the *a* axis (b).

is a mixed-valence selenium oxide, containing $Se^{IV}O_3$ triangular pyramids and $Se^{VI}O_4$ tetrahedra simultaneously.

To elucidate the structure more clearly, the bonds of Ag(2) and Ag(3) were left out. The backbone of **1** can be described as a 3D network consisting of silver/mercury selenite layers bridged by selenate tetrahedra (Fig. 1). Two $Ag/Hg(1)O_6$ octahedra were edge-shared into a $(Ag/Hg)_2O_9$ dimer (Fig. S4b), which were brought together by quadridentate $Se(1)O_3$ and $Se(2)O_3$ ligands into a 2D silver/mercury selenite layers parallel to (010) plane (Fig. 1a). The $Se(3)O_4$ tetrahedra bridged the silver/mercury selenite layers further to a 3D framework with $(Ag/Hg)_4(Se^{IV})_2(Se^{VI})_2$ eight-member polyhedral ring (MPR) tunnels along the *a* axis (Fig. 1b). The Ag(2) cations were located at the central of the 8-MPR tunnels while the Ag(3) cations were placed in the $(Ag/Hg)_4(Se^{VI})_3$ seven-member polyhedral rings of silver/mercury selenate layers formed by $(Ag/Hg)_2O_9$ dimers and $Se(3)O_4$ tetrahedra (Fig. S7). Interestingly, two other 1D tunnels were found along *b* and *c* axis of the structure. The small tunnels housing only Ag(2) cations were based on $(Ag/Hg)_2(Se^{IV})_2$ four-member polyhedral rings while Ag(3) cations were composed of $(Ag/Hg)_4(Se^{VI})_2$ six-member polyhedral rings (Fig. S8). So, **1** features a 3D open framework with eight-, four- and six-member polyhedral ring tunnels along *a*, *b* and *c* axes respectively.

### Crystal structure of $Ag_2Bi_2(SeO_3)_3(SeO_4)$ (2)

Compound **2** crystallizes in the central symmetric space group $P2_1/m$ (No. 11). Its asymmetric unit contains two silver, two bismuth, four selenium and nine oxygen, totaling 17 unique atoms. Ag(1) and Ag(2) are coordinated with three and four oxygen atoms respectively with the Ag–O distances in the range of 2.29(2)–2.580(9) Å (Fig. S9). Bi(1) and Bi(2) cations are seven coordinated with oxygen atoms in the $BiO_7$ monocapped trigonal prisms with the Bi–O bond lengths ranging from 2.227(11) to 2.705(8) Å (Fig. S10). Se(1)–Se(3) cations are in the $SeO_3$ triangular pyramid coordination with Se–O bond lengths in the range of 1.665(13)–1.72(2) Å while Se(4) is in a $SeO_4$ tetrahedral geometry with the Se–O bonds limited in 1.617(15)–1.622(9) Å, which are consistent with those in **1**. Bond valence calculations of Ag(1)–Ag(2), Bi(1)–Bi(2), Se(1)–Se(3) and Se(4) give the results of 0.44–0.78, 2.83–2.93, 4.03–4.17 and 6.29 (Table S2), respectively, proving that the oxidation states of Ag(1)–Ag(2), Bi(1)–Bi(2), Se(1)–Se(3) and Se(4) are +1, +3, +4 and +6, respectively [43,44]. The deviations of Ag(1) from the ideal oxidation can be attributed to their weak coordination bonds. If the Ag···O distances in the range of 2.7–3.0 Å are considered, the BVSs of the Ag(1) atoms are 0.74 [45–49].

The structure of compound **2** features a novel 3D bismuth selenite framework with 12- and 6-MPR tunnels along *b* axis (Fig. 2). The $Bi(1)O_7$ and $Bi(2)O_7$ polyhedra were edge-shared [O(3)···O(3)] to a $[Bi_2O_{12}]^{18-}$ dimer, which were bridged by $Se(1)O_3$ groups to a bismuth selenite double chain (Fig. 2a). The $Se(2)O_3$ groups linked the double chains to a 2D layer paralleled to (101) plane, which were further connected by the $Se(3)O_3$ groups to a 3D network (Fig. 2b, c). Big $Bi_6Se_6$ 12-MPR and small $Bi_3Se_3$ 6-MPR tunnels were formed in this bismuth selenite structure (Fig. 2c). Two $Se(4)O_4$ tetrahedra were attached on the internal walls of the big 12-MPR tunnels (Fig. 2d). Ag(1) and Ag(2) were situated in the 12- and 6-MPR tunnels respectively (Fig. 2d). The $Se(1)O_3$, $Se(3)O_3$ and $Se(4)O_4$ groups are tridentate, bridging with three

  

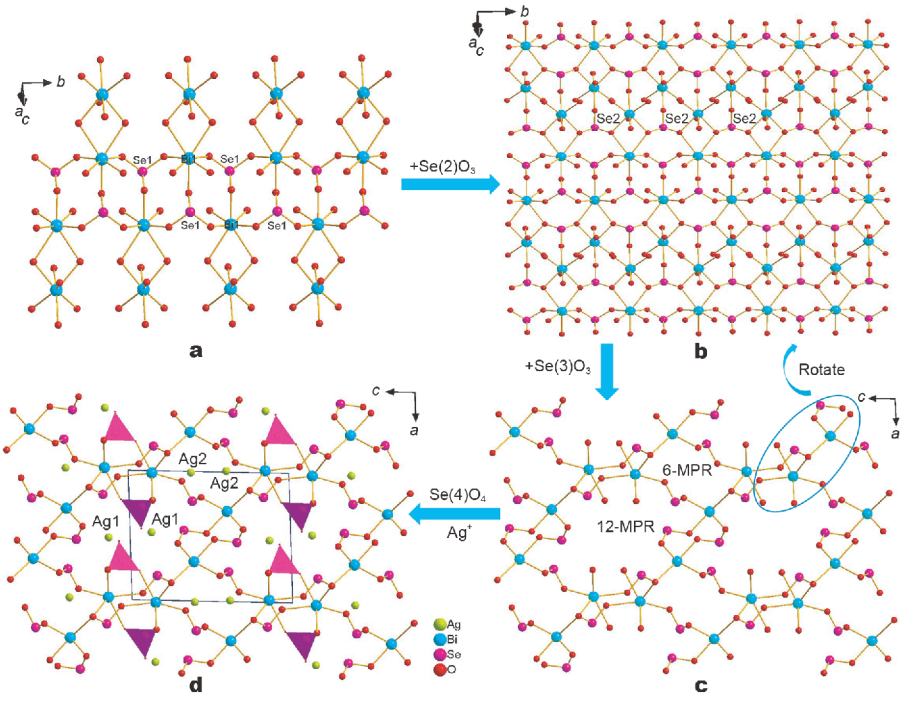


**Figure 2** Bismuth selenite double chain (a), 2D bismuth selenite layer parallel to (101) plane (b), 3D bismuth selenite framework with 12- and 6-MPR tunnels along *b* axis (c), view of the structure of $Ag_2Bi_2(SeO_3)_3(SeO_4)$ along the *a* axis (d).

bismuth atoms while the $Se(2)O_3$ group is a pentadentate ligand, bridging with 2 Bi(1) and 3 Bi(2) atoms (Fig. S11).

**Crystal structure of $Ag_5Bi(SeO_3)_4$ (3)**

Compounds **3** crystallizes in the centrosymmetric space group $I4_1/a$ (No. 88). There are one bismuth, two silver, one selenium and three oxygen, totaling 7 unique atoms in its asymmetric unit with Bi(1) and Ag(2) located at the −4 symmetry. Bi(1) is eight-coordinated in a $BiO_8$ dodecahedron with Bi–O bonds in the range of 2.428(5)–2.505(6) Å (Fig. S12). Ag(1) and Ag(2) are both bonded to four oxygen atoms with Ag–O ranging from 2.292(5) to 2.440(7) Å (Fig. S13). Se(1) is linked with three oxygen atoms in the $SeO_3$ triangular pyramidal geometry with Se–O bond lengths in the range of 1.696(6)–1.707(5) Å. Bond-valence-sum (BVS) calculation results of Bi(1), Ag(1), Ag(2), and Se(1) are 2.91, 0.92, 0.77, and 4.03 (Table S2), respectively [43,44], indicating that the valence states of Bi, Ag and Se atoms are +3, +1 and +4, respectively.

$BiAg_5(SeO_3)_4$ (**3**) exhibits a new 3D network formed by $BiO_8$ and $SeO_3$ groups. The isolated $BiO_8$ polyhedra were bridged by pairs of bidentate $SeO_3$ groups to a 3D open framework with three different 1D tunnels along *a*, *b*, and *c*-axes. The square shaped helical tunnels along *c*-axis were based on eight-member rings composed of four $BiO_8$ polyhedra and four $SeO_3$ groups (Fig. 3) [50]. In Fig. S14, the small $Bi_2Se_2$ 4-MPR tunnels are occupied with Ag(1) cations while the large $Bi_3Se_3$ 6-MPR tunnels accommodate Ag(1) and Ag(2) cations. Each 6-MPR tunnel is surrounded by four 4-MPR tunnels and each 4-MPR tunnel bridges two 6-MPR tunnels.

In these three compounds, the $SeO_3$ selenite groups expanded the dimension of the structure effectively. However, the $SeO_4$ selenate groups only played a positive role in the structural dimension of **1**. In **2**, they just decorated the internal walls of the 12-MPR tunnels. It is worth mentioning that there are some characteristics in common in the open frameworks of **1** and **3**. They both contain four-, six-, and eight-member polyhedral ring tunnels along *a*, *b* and *c* axes. The difference is that, in compound **1**, the four- and six-MPR tunnels are along *b* and *c* axes respectively, while in compound **3,** they are both parallel to *a* and *b* axes. The compositions of the polyhedral rings are different too.

In the reported mixed valence selenium oxides, the $SeO_3$ selenite groups and the $SeO_4$ selenate tetrahedra are often isolated and linked by other polyhedra separately except for the diselenium pentoxide $Se_2O_5$, which is a 1D chain structure formed by corner-sharing of $SeO_3$ triangular pyramids and $SeO_4$ tetrahedra [29]. Furthermore,

  

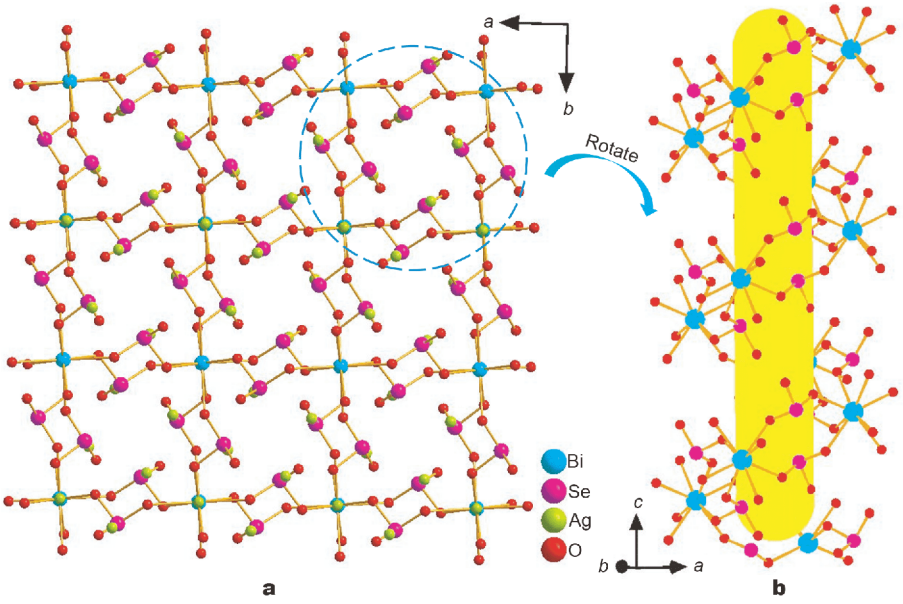


**Figure 3** View of the structure of $BiAg_5(SeO_3)_4$ along the *c* axis (a) and the bismuth selenite helical chain (b).

the coordination capabilities of $SeO_3$ groups are not weak compared with those of $SeO_4$ tetrahedra although the coordination number of selenium in selenite is lower than that in selenate. For example, only one hexadentate and one octadentate $SeO_4$ ligands were found in $Bi_2(SeO_3)_2(SeO_4)$ [27] and $Hg_4(HgO)(SeO_3)(SeO_4)$ [51], respectively. However, two examples of heptadentate $SeO_3$ groups were found in the structures of $Pr_4(SeO_3)_2(SeO_4)F_6$ [52] and $Hg_4(HgO)(SeO_3)(SeO_4)$. And octadentate $SeO_3$ ligands were also found in $Hg_3(SeO_3)_2(SeO_4)$ [25] and $Cd_3(SeO_3)_2(SeO_4)$ [53]. In most of the selenite-selenate compounds, the $SeO_3$ and $SeO_4$ groups bridge the cationic polyhedra to an expanded structure together [23–32].

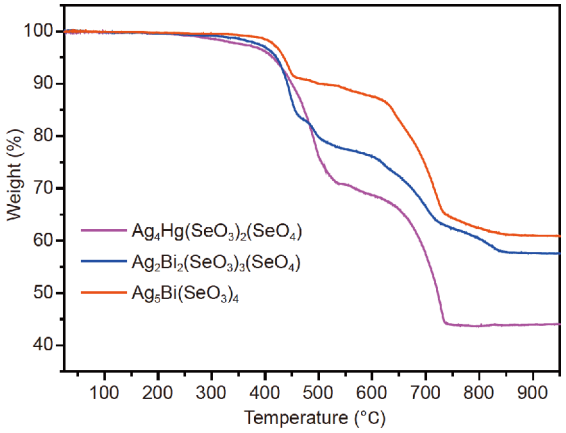


**Figure 4** TGA curves of compounds **1**–**3**.

### Optical measurements

The IR spectra for compounds **1**–**3** were measured in the wave number range of 4000–400 $cm^{-1}$ at 293 K (Fig. S15). All three compounds have no absorption in the range of 4000–900 $cm^{-1}$ and show strong characteristic peaks of $SeO_3^{2-}$ groups around 660 $cm^{-1}$ and 410–470 $cm^{-1}$. The strong bands at about 820 $cm^{-1}$ for compounds **1** and **2** can be assigned to the characteristic absorption of the $SeO_4^{2-}$ tetrahedra. These assignments are consistent with the data reported in the literature [23,32].

UV-vis-NIR absorption spectral analyses show that the three compounds are almost transparent from 2000 to 500 nm (Fig. S16). Their cutoff edges are 398, 339 and 346 nm respectively, corresponding to the optical band gaps of 3.11, 3.65, 3.58 eV for **1**, **2** and **3**, respectively. The absorption edge of compound **1** is significantly red shifted due to the doping of the transition metal $Hg^{2+}$ while the cutoff edge of compound **2** is slightly blue shifted because of the introduction of the $SeO_4$ tetrahedron.

### Thermal analyses

TGA of the three compounds have been studied in the range of 20–1000°C. As shown in Fig. 4, compounds **1**–**3** can be stable up to about 290, 340 and 400°C, respectively. After further heating, they showed significant weight loss. Compound **1** displays two main steps of weight loss in the temperature range of 290–740°C. These

  

weight losses correspond to the release of 3.0 $SeO_2$, 1.0 Hg vapor and 1.5 $O_2$ molecules. The observed weight loss of 56.3% is in coincidence with the calculated value of 56.5%. For compound **2**, the total weight loss of 41.3% between 330–850°C correspond to the release of 4.0 $SeO_2$ and 1.0 $O_2$ molecules per formula unit, which matches well with its calculated value of 41.1%. Compound **3** displays two main steps of weight losses. The first step corresponds to the loss of one molecule $SeO_2$ in the range of 370–455°C. The observed weight loss of 8.7% is very close to the calculated loss of 8.8%. The second weight loss in the temperature range of 455–840°C can be ascribed to the vaporization of 3.0 $SeO_2$ and 1.25 $O_2$ molecules. The observed weight loss of 30.3% is in coincidence with the calculated value of 29.7%.

### SHG properties of $Ag_4Hg(SeO_3)_2(SeO_4)$ (1)

SHG detection was performed on the sieved (70–100 mesh) crystalline sample of **1** since it crystalized in a noncentrosymmetric polar space group of $Cmc2_1$. Based on the UV-vis-NIR spectrum, this compound is transparent in the range of 500–2000 nm, so Q-switched Nd:YAG 1064 nm laser was chosen as the fundamental radiation. Fig. 5 shows that compound **1** displays a subtle SHG efficiency of approximately 35% times of that of commercial KDP, which further proves the NCS symmetry of the structure [54,55]. The weak SHG efficiency can be attributed to the opposite alignment of the selenite groups. The dipole moments of the $SeO_3^{2-}$ groups in **1** were calculated in Table S3. We can find that the *x*-components of the polarizations of the two $SeO_3$ units are zero, *y*-components of them are canceled out completely, and only small *z*-components are toward the same direction.

### Theoretical studies

Considering the severely disordered character of **1**, only the electronic properties of compounds **2** and **3** were calculated by CASTEP based on DFT methods. Their band structures along the high symmetry points of the first Brillouin zone are shown in Fig. 6. From the curves we can see that the two structures display different features. The top of valence bands (VBs) for the two compounds fluctuate moderately. The bottom of conduction bands (CBs) for compound **2** are more uneven than that for compound **3**. The state energies of the lowest conduction band (L-CB) and the highest valence band (H-VB) of the compounds are presented in Table S4. For compound **2**, the top of VBs is located at D point while the bottom of CBs is placed at B point. For **3**, the top of VBs is placed between N and G points while the bottom of CBs is located at N point. Hence, they all belong to indirect band gap compounds with theoretical band gaps of 2.91 and 2.42 eV, respectively, which are slightly smaller than the UV/vis results (3.65 and 3.58 eV). In DFT calculations band gaps are often underestimated because of the limitation of the GGA-PBE function. So, scissors of 0.74 and 1.16 eV were adopted for **2** and **3** in the following analyses [56].

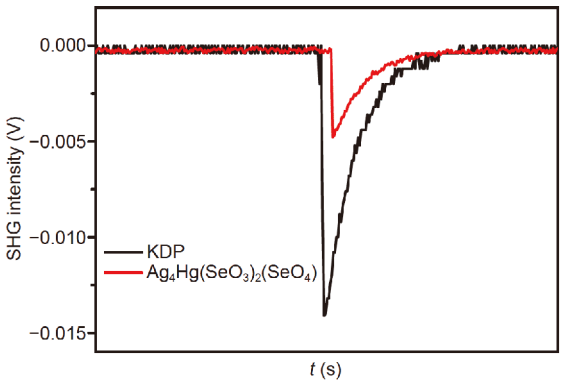


**Figure 5** Oscilloscope traces of the SHG signals for the sieved samples (70–100 mesh) of $Ag_4Hg(SeO_3)_2(SeO_4)$ and KDP.

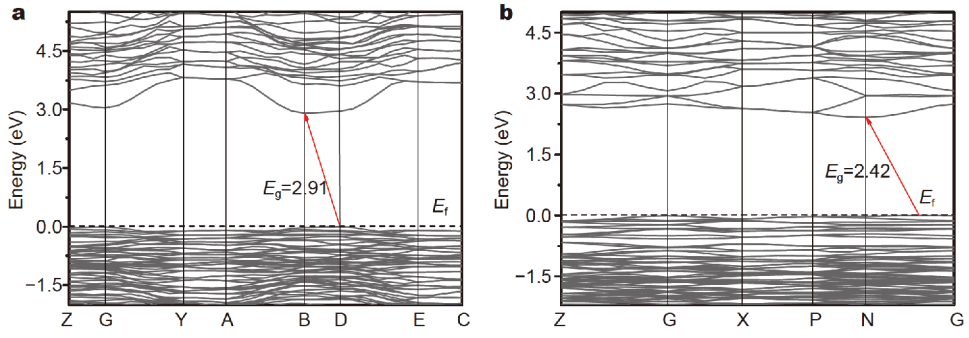


**Figure 6** The band structures of compounds **2** (a) and **3** (b).

  

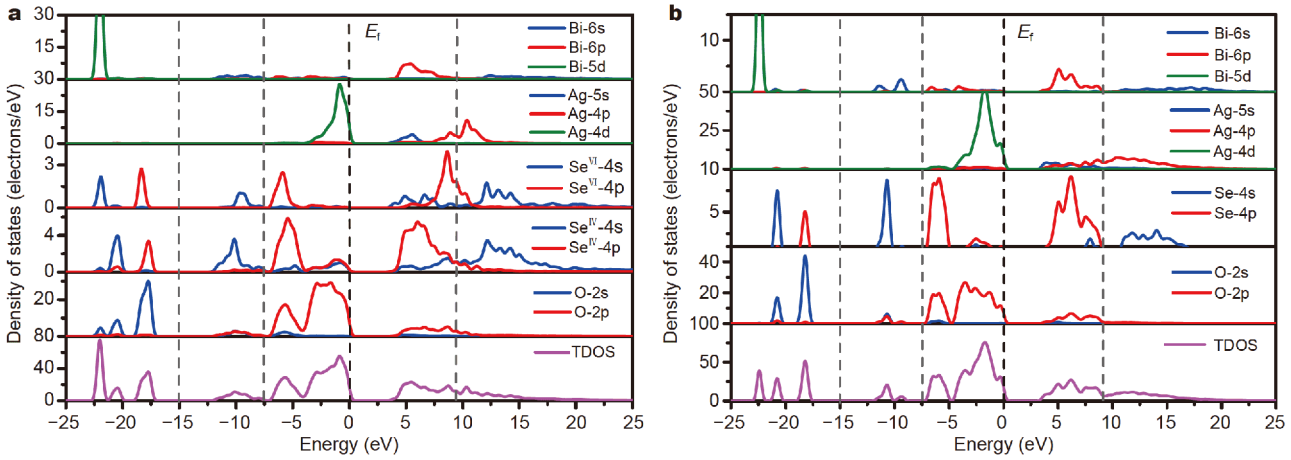


**Figure 7** The total and partial density of states (TDOS and PDOS) for compounds **2** (a) and **3** (b).

The total and partial density of states (TDOS and PDOS) for compounds **2** and **3** are shown in Fig. 7. The DOS of the two structures are generally similar except for the Se(VI) orbitals in compound **2**. Specifically, the VBs in the lower energy between −25.0 and −15.0 eV are constituted of Bi-5d, O-2s and Se-4s4p states. The peaks around −10 eV come from Se-4s and O-2s2p states mainly. The VBs near Fermi level (–7.5–0 eV) are made up of O-2p, Ag-4d and Se-4p states mostly. As for the CBs, the energy above 9.0 eV include the unoccupied Ag-4p and Se-4s states, while the lower portion (< 9.0 eV) is dominated by the empty O-2p, Bi-6p, Ag-5s and Se-4s4p orbitals. The O-2p and Ag-4d nonbonding orbitals consist of the highest VB [57], and the lowest CB originate from the Ag-5s, Bi-6p, Se-4p (and $Se^{VI}$-4s in compound **2**) and O-2p states. So, the band gaps of **2** and **3** are determined by Ag, Bi, Se and O atoms.

## CONCLUSIONS

Two new selenate-selenites, namely, $Ag_4Hg(SeO_3)_2(SeO_4)$ (**1**) and $Ag_2Bi_2(SeO_3)_3(SeO_4)$ (**2**), as well as a novel selenite of $Ag_5Bi(SeO_3)_4$ (**3**) have been synthesized successfully by *in-situ* hydrothermal reactions. We found that high temperature and oxidants were required for preparation of mixed-valence selenium oxides by selenium dioxide directly. They feature three different 3D networks with silver atoms situated in the space of the structures. Compound **1** is composed of silver/mercury selenite layers bridged by $SeO_4$ tetrahedra. Compound **2** is made up of 3D bismuth selenite with 12- and 6-MPR tunnels along *a* and *b* axes. Compound **3** is formed by the interconnection of $BiO_8$ and $SeO_3$ groups. Compound **1** crystallized in a NCS space group and displayed a subtle frequency doubling efficiency about 35% of KDP. This study revealed that selenate-selenites, containing $SeO_3$ triangular pyramids and $SeO_4$ tetrahedra simultaneously, could create novel NCS structures and exhibit interesting SHG properties. Next, we will make our efforts on preparation of other new metal selenate-selenites.

**Received 3 September 2019; accepted 23 September 2019; published online 22 October 2019**


1 Shi G, Wang Y, Zhang F, *et al.* Finding the next deep-ultraviolet nonlinear optical material: $NH_4B_4O_6F$. J Am Chem Soc, 2017, 139: 10645–10648
2 Kang L, Zhang X, Liang F, *et al.* Poly(difluorophosphazene) as the first deep-ultraviolet nonlinear optical polymer: a first-principles prediction. Angew Chem Int Ed, 2019, 58: 10250–10254
3 Guo SP, Chi Y, Xue HG. $SnI_4{\cdot}(S_8)_2$: A novel adduct-type infrared second-order nonlinear optical crystal. Angew Chem Int Ed, 2018, 57: 11540–11543
4 Xie Z, Wang Y, Cheng S, *et al.* Synthesis, characterization, and theoretical analysis of three new nonlinear optical materials $K_7MRE_2B_{15}O_{30}$ (M= Ca and Ba, RE= La and Bi). Sci China Mater, 2019, 62: 1151–1161
5 Kim SH, Yeon J, Halasyamani PS. Noncentrosymmetric polar oxide material, $Pb_3SeO_5$: synthesis, characterization, electronic structure calculations, and structure−property relationships. Chem Mater, 2009, 21: 5335–5342
6 Bang S, Ok KM. Structure-directing effect of alkali metal cations in new molybdenum selenites, $Na_2Mo_2O_5(SeO_3)_2$, $K_2Mo_2O_5(SeO_3)_2$, and $Rb_2Mo_3O_7(SeO_3)_3$. Inorg Chem, 2015, 54: 8832–8839
7 Xia Z, Poeppelmeier KR. Chemistry-inspired adaptable framework structures. Acc Chem Res, 2017, 50: 1222–1230
8 Harrison WTA, Dussack LL, Jacobson AJ. Syntheses, crystal structures, and properties of new layered molybdenum(VI) selenites: $(NH_4)_2(MoO_3)_3SeO_3$ and $Cs_2(MoO_3)_3SeO_3$. Inorg Chem, 1994, 33: 6043–6049
9 Nguyen SD, Kim SH, Halasyamani PS. Synthesis, characterization, and structure–property relationships in two new polar oxides:


  

$Zn_2(MoO_4)(SeO_3)$ and $Zn_2(MoO_4)(TeO_3)$. Inorg Chem, 2011, 50: 5215–5222
10 Cao XL, Hu CL, Xu X, *et al.* $Pb_2TiOF(SeO_3)_2Cl$ and $Pb_2NbO_2(SeO_3)_2Cl$: small changes in structure induced a very large SHG enhancement. Chem Commun, 2013, 49: 9965–9967
11 Liang ML, Hu CL, Kong F, *et al.* $BiFSeO_3$: An excellent SHG material designed by aliovalent substitution. J Am Chem Soc, 2016, 138: 9433–9436
12 You F, Liang F, Huang Q, *et al.* $Pb_2GaF_2(SeO_3)_2Cl$: band engineering strategy by aliovalent substitution for enlarging bandgap while keeping strong second harmonic generation response. J Am Chem Soc, 2019, 141: 748–752
13 Ma YX, Hu CL, Li BX, *et al.* $PbCdF(SeO_3)(NO_3)$: A nonlinear optical material produced by synergistic effect of four functional units. Inorg Chem, 2018, 57: 11839–11846
14 Yu H, Nisbet ML, Poeppelmeier KR. Assisting the effective design of polar iodates with early transition-metal oxide fluoride anions. J Am Chem Soc, 2018, 140: 8868–8876
15 Zhang X, Wu H, Yu H, *et al.* $Ba_4M(CO_3)_2(BO_3)_2$ (M=Ba, Sr): two borate-carbonates synthesized by open high temperature solution method. Sci China Mater, 2019, 62: 1023–1032
16 Yu H, Koocher NZ, Rondinelli JM, *et al.* $Pb_2BO_3I$: a borate iodide with the largest second-harmonic generation (SHG) response in the $KBe_2BO_3F_2$ (KBBF) family of nonlinear optical (NLO) materials. Angew Chem Int Ed, 2018, 57: 6100–6103
17 Dong X, Huang L, Hu C, *et al.* $CsSbF_2SO_4$: an excellent ultraviolet nonlinear optical sulfate with a $KTiOPO_4$ (KTP)-type structure. Angew Chem Int Ed, 2019, 58: 6528–6534
18 Lee DW, Bak D, Kim SB, *et al.* Effect of the framework flexibility on the centricities in centrosymmetric $In_2Zn(SeO_3)_4$ and noncentrosymmetric $Ga_2Zn(TeO_3)_4$. Inorg Chem, 2012, 51: 7844–7850
19 Kong F, Huang SP, Sun ZM, *et al.* $Se_2(B_2O_7)$: a new type of second-order NLO material. J Am Chem Soc, 2006, 128: 7750–7751
20 Kong F, Xu X, Mao JG. A series of new ternary and quaternary compounds in the $Li^{I}$–$Ga^{III}$–$Te^{IV}$–O system. Inorg Chem, 2010, 49: 11573–11580
21 Gong YP, Ma YX, Ying SM, *et al.* Two indium sulfate tellurites: centrosymmetric $In_2(SO_4)(TeO_3)(OH)_2(H_2O)$ and non-centrosymmetric $In_3(SO_4)(TeO_3)_2F_3(H_2O)$. Inorg Chem, 2019, 58: 11155–11163
22 He F, Wang L, Hu C, *et al.* Cation-tuned synthesis of the $A_2SO_4{\cdot}SbF_3$ (A = $Na^+$, $NH_4^+$, $K^+$, $Rb^+$) family with nonlinear optical properties. Dalton Trans, 2018, 47: 17486–17492
23 Morris RE, Wilkinson AP, Cheetham AK. A novel mixed-valence selenium(IV)/selenium(VI) oxo compound: crystal structure determination and X-ray absorption near edge structure study of erbium selenite(IV) selenate(VI) hydrate, $Er(SeO_3)(SeO_4)_{1/2}{\cdot}H_2O$. Inorg Chem, 1992, 31: 4774–4777
24 Weil M. The crystal structures of $Hg_7Se_3O_{13}H_2$ and $Hg_8Se_4O_{17}H_2$—two mixed-valent mercury oxoselenium compounds with a multifarious crystal chemistry. Z für Kristallographie-Crystline Mater, 2004, 219: 621–629
25 Weil M, Kolitsch U. $Hg_3Se_3O_{10}$, a mercury(II) compound with mixed-valence oxoselenium(IV/VI) anions. Acta Cryst, 2002, 58: i47–i49
26 Wickleder MS, Büchner O, Wickleder C, *et al.* $Au_2(SeO_3)_2(SeO_4)$: Synthesis and characterization of a new noncentrosymmetric selenite−selenate. Inorg Chem, 2004, 43: 5860–5864
27 Lee EP, Song SY, Lee DW, *et al.* New bismuth selenium oxides: syntheses, structures, and characterizations of centrosymmetric $Bi_2(SeO_3)_2(SeO_4)$ and $Bi_2(TeO_3)_2(SeO_4)$ and noncentrosymmetric $Bi(SeO_3)(HSeO_3)$. Inorg Chem, 2013, 52: 4097–4103
28 Baran J, Lis T, Marchewka M, *et al.* Structure and polarized IR and Raman spectra of $Na_2SeO_4{\cdot}H_2SeO_3{\cdot}H_2O$ crystal. J Mol Structure, 1991, 250: 13–45
29 Zak Z. Crystal structure of diselenium pentoxide $Se_2O_5$. Z Anorg Allg Chem, 1980, 460: 81–85
30 Giester G. Crystal structure of $Li_2Cu_3(SeO_3)_2(SeO_4)_2$. Monatshefte für Chemie, 1989, 120: 661–666
31 Effenberger H. Crystal structure and chemical formula of schmiederite, $Pb_2Cu_2(OH)_4(SeO_3)(SeO_4)$, with a comparison to linarite, $PbCu(OH)_2(SO_4)$. Miner Petrol, 1987, 36: 3–12
32 Ling J, Albrecht-Schmitt TE. Syntheses, structures, and properties of $Ag_4(Mo_2O_5)(SeO_4)_2(SeO_3)$ and $Ag_2(MoO_3)_3SeO_3$. J Solid State Chem, 2007, 180: 1601–1607
33 Maggard PA, Nault TS, Stern CL, *et al.* Alignment of acentric $MoO_3F_3^{3-}$ anions in a polar material: $(Ag_3MoO_3F_3)(Ag_3MoO_4)Cl$. J Solid State Chem, 2003, 175: 27–33
34 Qian Q, Kong F, Mao JG. A series of new silver selenites with $d^0$-TM cations. RSC Adv, 2016, 6: 79681–79687
35 Gong YP, Hu CL, Kong F, *et al.* Exploration of new birefringent crystals in bismuth $d^0$ transition metal selenites. Chem Eur J, 2019, 25: 3685–3694
36 Wu BL, Hu CL, Mao FF, *et al.* Highly polarizable $Hg^{2+}$ induced a strong second harmonic generation signal and large birefringence in $LiHgPO_4$. J Am Chem Soc, 2019, 141: 10188–10192
37 Shi S, Luo M, Lin C, *et al.* A cation size effect on the framework structures in $ABi_2SeO_3F_5$ (A = K and Rb): first examples of alkali metal bismuth selenite fluorides. Dalton Trans, 2018, 47: 6598–6604
38 Kurtz SK, Perry TT. A powder technique for the evaluation of nonlinear optical materials. J Appl Phys, 1968, 39: 3798–3813
39 Anonymous. Crystal Clear, version 1.3.5, Rigaku Corp, Woodlands, TX, 1999
40 Sheldrick GM. SHELXTL: crystallographic software package, version 5.1, Bruker-AXS, Madison, WI, 1998
41 Spek AL. Single-crystal structure validation with the program PLATON. J Appl Crystlogr, 2003, 36: 7–13
42 Segall MD, Lindan PJD, Probert MJ, *et al.* First-principles simulation: ideas, illustrations and the CASTEP code. J Phys-Condens Matter, 2002, 14: 2717–2744
43 Brese NE, O'Keeffe M. Bond-valence parameters for solids. Acta Crystlogr B Struct Sci, 1991, 47: 192–197
44 Brown ID, Altermatt D. Bond-valence parameters obtained from a systematic analysis of the Inorganic Crystal Structure Database. Acta Crystlogr B Struct Sci, 1985, 41: 244–247
45 Zhou Y, Hu CL, Hu T, *et al.* Explorations of new second-order NLO materials in the $Ag^{I}$-$Mo^{VI}$/$W^{VI}$-$Te^{IV}$-O systems. Dalton Trans, 2009, 102: 5747–5754
46 Poe TN, White FD, Proust V, *et al.* $[Ag_2M(Te_2O_5)_2]SO_4$ (M = $Ce^{IV}$ or $Th^{IV}$): A new purely inorganic d/f-heterometallic cationic material. Inorg Chem, 2018, 57: 4816–4819
47 Schmaltz B, Jouaiti A, Hosseini MW, *et al.* Double stranded interwound infinite linear silver coordination network. Chem Commun, 2001, 14: 1242–1243
48 Lian ZX, Cai J, Chen CH, *et al.* Linear silver isonicotinamide complex extended by arenedisulfonate *via* hydrogen bonds and weak Ag···O interactions. CrystEngComm, 2007, 9: 319–327
49 Khlobystov AN, Blake AJ, Champness NR, *et al.* Supramolecular design of one-dimensional coordination polymers based on

  

silver(I) complexes of aromatic nitrogen-donor ligands. Coord Chem Rev, 2001, 222: 155–192
50 Ma YX, Gong YP, Hu C, *et al.* Three new $d^{10}$ transition metal selenites containing $PO_4$ tetrahedron: $Cd_7(HPO_4)_2(PO_4)_2(SeO_3)_2$, $Cd_6(PO_4)_{1.34}(SeO_3)_{4.66}$ and $Zn_3(HPO_4)(SeO_3)_2(H_2O)$. J Solid State Chem, 2018, 262: 320–326
51 Weil M, Shirkanlou M. Hydrothermal Studies in the system Hg/Se/Te/O: The first $Te^{IV}/Se^{VI}$ oxocompounds $Hg_3SeTe_2O_{10}$ and $Hg_3SeTe_4O_{14}$, and the Mixed-valent $Hg_5Se_2O_8$. Z Anorg Allg Chem, 2015, 641: 1459–1466
52 Ina Krügermann, Wickleder MS. $Pr_4(SeO_3)_2(SeO_4)F_6$ and NaSm$(SeO_3)(SeO_4)$: selenite-selenates of rare earth elements. Z Anorg Allg Chem, 2002, 628: 147–151
53 Weil M. $Cd_3Se_3O_{10}$, isotypic with its mercury analogue. Acta Cryst, 2002, 58: i127–i129
54 Wu H, Yu H, Yang Z, *et al.* Designing a deep-ultraviolet nonlinear optical material with a large second harmonic generation response. J Am Chem Soc, 2013, 135: 4215–4218
55 Mutailipu M, Zhang M, Zhang B, *et al.* $SrB_5O_7F_3$ functionalized with $[B_5O_9F_3]^{6-}$ chromophores: accelerating the rational design of deep-ultraviolet nonlinear optical materials. Angew Chem Int Ed, 2018, 57: 6095–6099
56 Gong P, Liang F, Kang L, *et al.* Recent advances and future perspectives on infrared nonlinear optical metal halides. Coord Chem Rev, 2019, 380: 83–102
57 Xu X, Hu CL, Li BX, *et al.* α-$AgI_3O_8$ and β-$AgI_3O_8$ with large SHG responses: polymerization of $IO_3$ groups into the $I_3O_8$ polyiodate anion. Chem Mater, 2014, 26: 3219–3230

**Acknowledgements** This work was supported by the National Natural Science Foundation of China (21773244 and 21875248), the Strategic Priority Research Program of the Chinese Academy of Sciences (XDB20000000), and the Natural Science Foundation of Fujian Province (2018J01025).

**Author contributions** Wang XX performed the experiments and data analysis, and wrote the first draft of the paper; Li XB gave assistance on the data analysis, Hu CL performed the theoretical data analysis; Kong F and Mao JG supervised the experiments and revised the manuscript. All authors contributed to the general discussion.

**Conflict of interest** The authors declare that they have no conflict of interest.

**Supplementary information** Supporting data are available in the online version of the paper.

**Xiaoxue Wang** received her Bachelor degree in chemistry at the Department of Chemistry and Chemical Engineering of Liaocheng Universtiy. She is currently a Master candidate of the Department of Chemistry at Fuzhou University and Fujian Institute of Research on the Structure of Matter (FJIRSM), Chinese Academy of Sciences (CAS) under the supervision of Prof. Fang Kong. Her research focuses on the synthesis, structure and characterization of new non-centrosymmetric materials based on metal selenites or tellurites.

**Fang Kong** received her PhD degree on inorganic chemistry from FJIRSM, CAS under the direction of Prof. Jianggao Mao. Then she joined the faculty of FJIRSM as an Assistant Professor and is currently a Full Professor. She is a member of Youth Innovation Promotion Association of CAS. Her research interest is focused on new SHG materials based on oxyanions of lone pair cations.

**Jiang-Gao Mao** received his PhD from Changchun Institute of Applied Chemistry, CAS under the supervision of Professor Jiazuan Ni (Academician). He did post-doctoral research at FJIRSM, Chinese University of Hong Kong, University of Houston and Texas A&M University from 1994 to 2002. Since 2002, he has been working as a full professor at FJIRSM, CAS. His current research interest includes the design, syntheses, and crystal structures of new functional inorganic solids, especially NLO materials.

## $Ag_4Hg(SeO_3)_2(SeO_4)$:原位合成法制备的混价硒氧化物类新型倍频材料

王晓雪[1,2], 李小宝[1,2], 胡春丽[2], 孔芳[2*], 毛江高[2*]

**摘要** 我们在$Ag^+$-$Hg^{2+}$/$Bi^{3+}$-$SeO_3^{2-}$体系探索合成新型非线性光学材料时获得了三例结构新颖的银硒氧化物: $Ag_4Hg(SeO_3)_2(SeO_4)$ (**1**), $Ag_2Bi_2(SeO_3)_3(SeO_4)$ (**2**) 和 $Ag_5Bi(SeO_3)_4$ (**3**). 它们展现了丰富的晶体化学: **1**和**2**为同时含六价和四价硒的混价氧化物; **1**和**3**为在*a*、*b*或*c*轴含四、六或八元环孔道的三维开放式骨架结构; **1**结晶于非心和极性空间群, 并且可以显示出明显的倍频信号, 约为商用KDP的35%. 紫外漫反射光谱表明这三例化合物均为宽带隙半导体, 其光学带隙分别为3.11、3.65和3.58 eV. 理论计算发现材料**2**和**3**为间接带隙半导体, 其带隙是由Ag、Bi、Se和O原子共同决定的.

  